

Project 980: Tomographic imaging of the Askja magma chamber and magmatic seismicity under Vatnajökull, Iceland

Abstract

The original objectives of this proposal were

1. To make a tomographic image of the low-velocity, hot or/or melt-bearing bodies beneath Askja central volcano in the northern rift zone of Iceland;
2. To constrain the crustal and upper mantle velocity structure, including anisotropy beneath the northern rift zone and the Vatnajökull region using ambient noise and surface waves;
3. To map seismicity caused by melt movement beneath the five active volcanoes currently lying beneath the Vatnajökull ice cap.

All three objectives have been achieved, and published, with more papers in preparation. A separate scientific report (loan 968) covers the first objective. To save repetition, I here report on the last two objectives. Loan 980 of 20 seismometers supplemented 26 6TD and ESP seismometers purchased by Cambridge University and deployed on this project. During summer 2014 to summer 2015 the array was also supplemented by 15 Guralp 6TDs from SEIS-UK under loan 1022 extension deployed to monitor the Holuhraun eruption.

Background

Tomographic imaging of volcanoes is an important tool in understanding the distribution of melt below the surface because molten rock strongly reduces the seismic velocity. S-waves are especially sensitive to temperatures and the presence of melt because S-waves cannot travel through liquid. Even small percentages of melt will change the bulk properties and depress the seismic velocity. We used ambient noise to constrain the shear velocity structure beneath Iceland.

Seismicity caused by melt movement along a 48 km long dyke during the Bardarbunga – Holuhraun intrusion and eruption was captured spectacularly well by our array. We have also identified and mapped a vertical melt feed from 20 km deep in the crust up to the depth of the dyke. Vatnajökull is located above the central part of the Eastern rift zone in Iceland. This marks the location of the plate spreading boundary between the North American and Eurasian plates where it passes through Iceland.

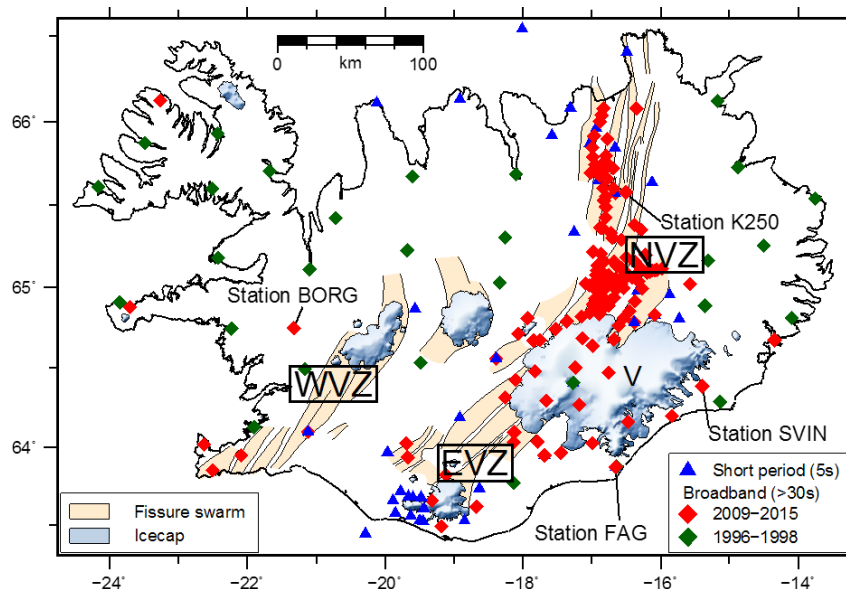
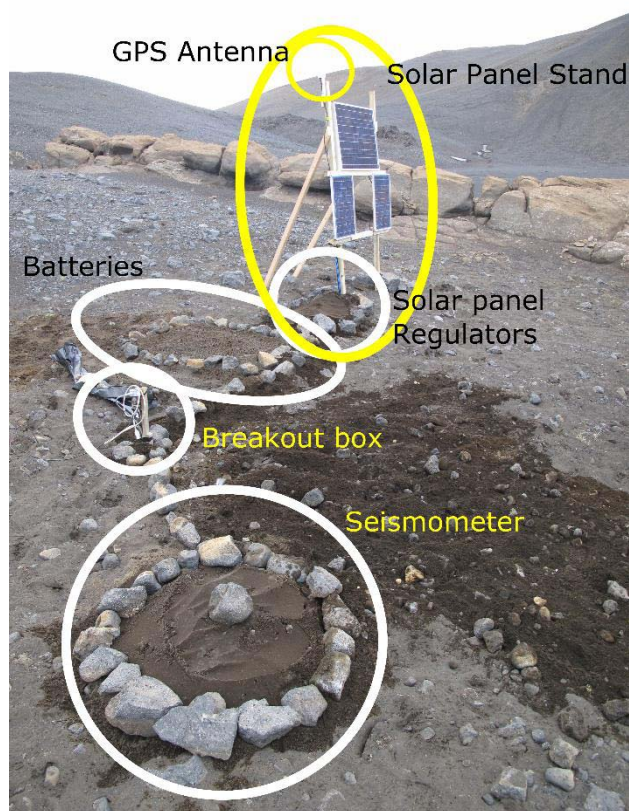


Figure 1. Icelandic fissure swarms in beige make up the 3 rift zones; the northern, eastern and western volcanic zones (NVZ, EVZ, WVZ). Broadband seismometers from the Cambridge deployments (and additional permanent IMO stations) are the red diamonds concentrated in the rift zones and around the volcanically active Vatnajökull region (V). Green diamonds show HOTSPOT broadband stations, blue triangle mark short period seismometers.

Survey procedure



The seismic data was recorded continuously at 100 sps with continuous GPS. Almost continuous daylight in summer (this is near the Arctic circle), together with the use of large truck batteries (typically 3 x 115 Amp-hrs) and multiple solar panels on each site (typically 80 watts), provided sufficient power supply through both the summer and winter months to keep the seismometers operating continuously. Solar panels are mounted sub-vertically to reduce snow adherence in the wetter spring months and to catch the low angle returning sun (Fig. 2). The GPS antenna is attached to the top of the stand so that it is above the snow cover. We bury the batteries and solar panel regulators, but mount the breakout box on a short stick: this is because when they are buried, they are more prone to becoming flooded as the snow melts. It is also easier to access the sockets for servicing. 6TD seismometers were buried directly (in plastic bags), while for ESPs we built a small underground vault using fish barrels and concreted base, with drainage (Fig. 3).

Figure 2. Typical deployment method in Iceland.

The prevalence of basaltic rocks means that compasses are unreliable indicators of true north, so we used GPS to orient the seismometers. It is best to use a differential GPS receiver, but when that was not available we found that a normal hand-held GPS unit could be used equally well. We took a fix at the seismometer and then walked quickly 100-200 metres either north or south (depending on the terrain) and erected a pole at that point to provide a visual pointer for aligning the seismometer. At these high latitudes there is excellent satellite coverage, and provided little time was spent in locating the position for the pointer (by simply keeping the longitude on the GPS the same as you walked), the normal time-varying positional errors in the GPS were minimised to less than the practical accuracy of aligning the seismometer.

Fig. 3 Installation in a buried fish barrel with sawn off and concreted base. Usually used for ESPs. Note that cable exit is below the top of the seismometer to prevent water running down cables, and a watertight lid is clamped on top. We did not add insulation or other packing round the seismometer.



A 16 Gbyte seismometer typically filled the memory in 10.5 months, so we serviced the array twice: once in early July, which is the earliest we could access the area; and again in early September. This also gave us the opportunity to replace any failing components at the sites (we found the GPS antennae to be often the most likely component to fail during deployments).

The ambient noise tomography across Vatnajökull required multiple crossing ray-paths. Figure 4 shows the seismometer array used for the tomography during its peak period in 2014-15. An advantage of the ambient noise method is that paths between pairs of receivers can simply be added into the final stacks without requiring the whole array to be operational simultaneously.

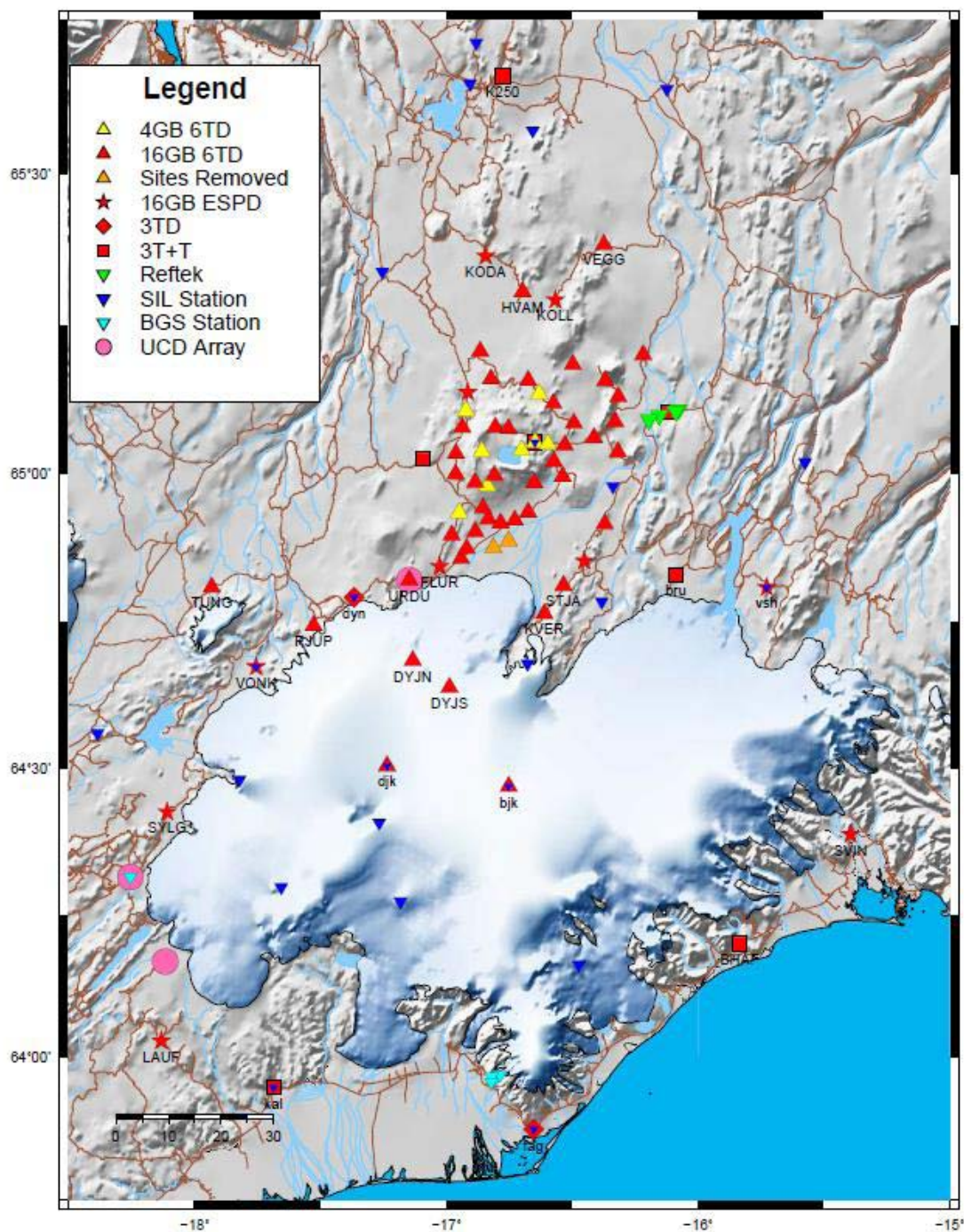


Figure 4. Seismic network from September 2014 to July 2015. Brown and blue lines show gravel roads and rivers respectively.

Data quality

The data quality is extremely good, particularly in the winter. This is because the ground is frozen, so the buried seismometers are coupled to the ground extremely well. There is no cultural noise, and the lack of vegetation means that there is no noise induced, for example by wind blowing trees. The snow cover decouples the ground somewhat from wind shear.

Processing and modelling

This multi-network ambient noise tomography study uses continuous broadband seismic data from a total of 232 (non-simultaneous) seismic stations across Iceland (Figure 1). 144 stations are part of an ongoing deployment in central and east Iceland, operated by the University of Cambridge and University of Iceland, and this array is augmented by 48 permanent sites from the monitoring network of the Icelandic Meteorological Office (IMO), and 3 sites from the IMAGE project Reykjanes Ridge experiment. To supplement this, additional archive data from a summer deployment at Eyjafjallajökull volcano and the HOTSPOT experiment of 1996–98 [25] were collated and reprocessed to extend coverage to the margins of Iceland.

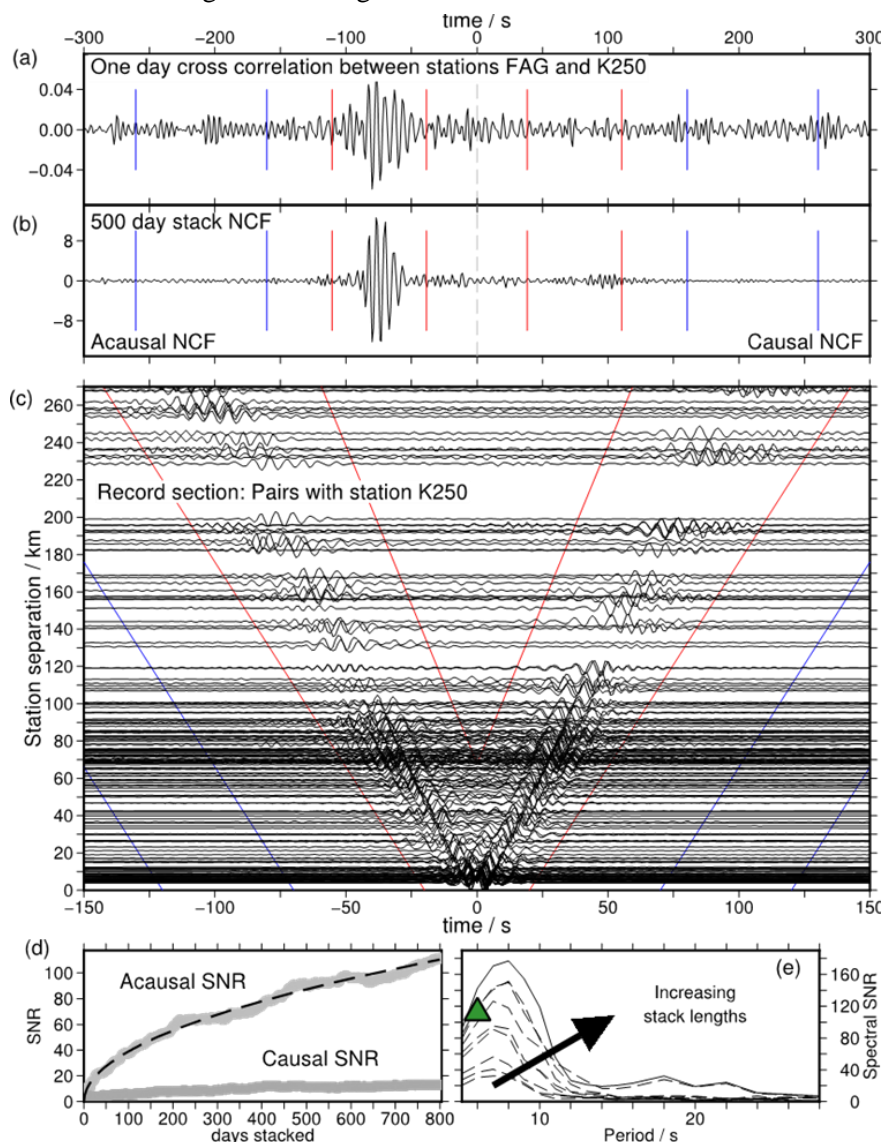


Figure 5. Extraction of Rayleigh waves. (a) 1-day Noise Correlation Function (NCF). (b) 500-day stacked NCF for the same station pair. (c) record section for pairs with station K250. Red lines show signal window and blue lines show noise window for SNR calculations. (d) SNR emergence with length of stack. (e) Spectral SNR for stacks of 30, 60, 100, 200, 300, 400, 500, 600 and 800 days. Green triangle marks the broadband SNR.

Ambient noise analysis involves the cross correlation of long term seismic noise to reconstruct a Noise Correlation function (NCF) which is an estimate of the earth response between two stations.

Wavespeed observations, most commonly surface wave dispersion, are then measured for interstation NCFs and used to determine tomographic velocity maps. Our methods are similar to those laid out in

Bensen et al. (2007). Continuous vertical component records at 1 Hz sampling rate were split into day-long records, and then demeaned, detrended and tapered and the instrument response was removed to displacement. The mean station pair data record length was 390 days, with 755 pairs having data records longer than 2 years.

Interpretation of ambient noise tomography [see Green et al., 2017 for full details]

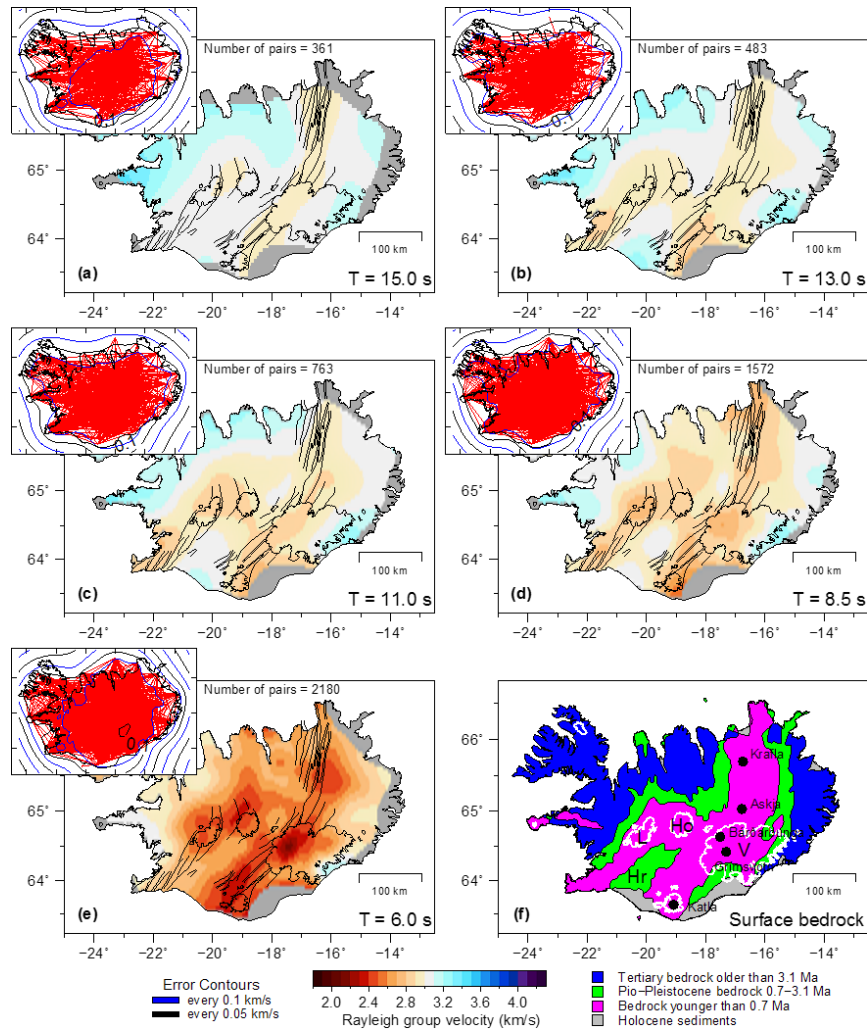


Figure 6. Rayleigh wave group velocity maps at 15–6 s period (a-e) and comparison to surface geology (f). Grey regions of the model are unconstrained. Black lines mark the rift systems and ice caps for reference. Inset maps show the ray path distribution as red lines. Blue and black lines display error contours every 0.1 and 0.05 km s^{-1} . (f) shows surface bedrock age. Crust younger than 0.7 Ma in (f) delineates the modern neo-volcanic zones.

The continuous band of low velocities constrain a 50 km wide rift. The most volcanically active regions show very low velocities, in particular beneath the Vatnajökull icecap, and the highly active Eastern Volcanic Zone. These regions must have been active for a relatively long time, as short-lived intrusion events for which we know the dates do not have an associated seismic velocity perturbation. The melt is likely to be widely distributed as low percentage melt, rather than large melt bodies. The distribution of earthquakes and seismic velocity anomalies beneath Askja (report 968) are suggestive of a complex magmatic plumbing system with melt distributed throughout the crust (Figure 6). Melt is currently being actively intruded into a number of discrete locations in the mid-crust, rather than at a single storage reservoir beneath the central volcano.

Interpretation of melt under Vatnajökull [see Hudson et al., 2017 and Ágústsdóttir et al, 2016 for full details and for movies in the Supplementary Information]

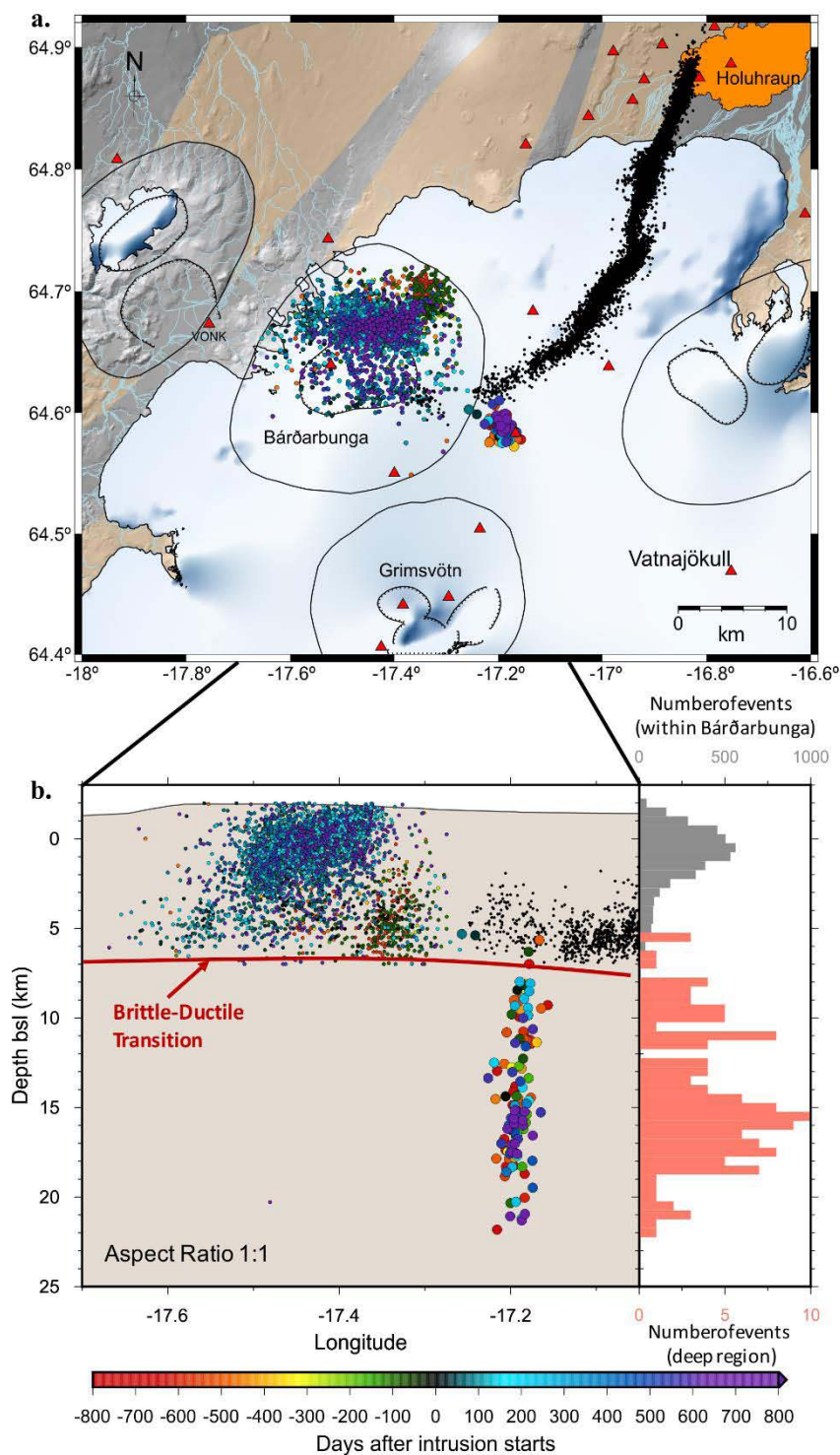


Figure 7. Map showing seismicity coloured by time after start of 2014-15 Bárðarbunga-Holuhraun dyke intrusion with intrusive period in black. (a) Sand coloured areas delineate fissure swarms, red triangles show seismic stations. (b) East-west vertical plane projection showing seismicity in (a) and the deep seismicity extending from 7-21 km depth. Histograms are for hypocentres in Bárðarbunga (grey) and deep events (red).

Over a 13 day period in 2014 magma propagated laterally from the sub-glacial Bárðarbunga volcano in the northern rift zone, Iceland. It created > 30,000 earthquakes at 5–7 km depth along a 48 km path before erupting on 29 August 2014 (black dots, Figure 7a). The seismicity, which tracked the dike propagation, advanced in short bursts at 0.3–4.7 km/h separated by pauses of up to 81 hours. During each surge forward, seismicity behind the dike tip dropped. Moment tensor solutions from the leading edge show exclusively left-lateral strike-slip faulting sub-parallel to the advancing dike tip, releasing

accumulated strain deficit in the brittle layer of the rift zone. Behind the leading edge, both left- and right-lateral strike-slip earthquakes are observed. The lack of non-double-couple earthquakes implies that the dike opening was aseismic.

We have also mapped the magma plumbing beneath Bardarbunga over a four year period 2013-2016 which encompasses the Holuhraun dyke intrusion and eruption. Microseismicity was recorded in a narrow sub-vertical column extending from 7-22 km depth (Figure 7b) (Hudson et al., 2017). Moment tensor solutions from these deep earthquakes exhibit opening tensile crack behaviour. This is consistent with the deep seismicity being caused by melt movement through the normally aseismic ductile crust. The seismically inferred melt path from the mantle source is offset laterally from the centre of the Bardarbunga caldera by ~12 km, rather than lying directly beneath it. It is likely that an aseismic melt feed supplies the shallow magma chamber at c. 7 km depth that lies directly beneath the caldera, and is aseismic due to the elevated temperatures and pervasive partial melt under the caldera.

Conclusions and recommendations

We have collected and assimilated a large dataset of continuous broadband seismic data for ambient noise analysis, and implemented a careful quality control procedure to remove poor quality data and to estimate uncertainty in the Rayleigh wave group velocities. Our high resolution model of the shear velocity structure of the Mid-Atlantic Ridge in Iceland displays an excellent spatial correlation of low seismic velocities within the active rift zones, and faster velocities in the older, cooler, less fractured, non-volcanically-active crust. This image reveals an oceanic rift with a continuous plumbing system feeding all three volcanic rift zones of the plate boundary in Iceland. Strong cores of the low-velocity anomalies are focussed under Katla and north-west Vatnajökull, and are possibly related to a broad region of partial melt under these large volcanic complexes, suggesting a concentrated delivery of melt into the crust at these locations. Shear wave velocity profiles of both on-rift and off-rift regions show a high velocity-gradient upper crust of 8–10 km thickness. Below this, shear velocities increase with a lower velocity-gradient, and in the on-rift region the crustal shear velocities are depressed between depths of 10–20 km.

Over 30,000 brittle failure earthquakes delineate the path of a 48 km lateral dyke beneath the Vatnajökull ice cap at 6 km depth feeding the Holuhraun eruption. A persistent feed of melt sub-vertically through the crust has been identified just outside the Bardarbunga caldera.

At the time of writing we are analysing the anisotropy of the crust from local and regional events and making a tomographic image of the magma chamber beneath Bardarbunga using P and S body wave arrivals.

Location of the archived data

The raw and miniseed data are archived at Bullard Laboratories, Cambridge University on two different RAID arrays in different buildings, and also at SEIS-UK. The data will be uploaded to IRIS in August 2019, 3 years after the end of the loan. In the meantime, we are collaborating and providing this data for research with several researchers in other countries (Germany, Belgium, Estonia, Iceland, Ireland and France).

The locations of all the microearthquakes we have identified are published in Supplementary Information of Ágústsdóttir et al. (2016) [approx. 30,000 events from the Bardarbunga dyke], in Greenfield et al. [approx. 70,000 events from the Askja-Herðubreið area], and in Hudson et al. (2017), where they are publicly available for download.

Text Citations

Bensen GD, Ritzwoller MH, Barmin MP, Levshin AL, Lin F, Moschetti MP, et al. Processing seismic ambient noise data to obtain reliable broad-band surface wave dispersion measurements. *Geophys J. Int.* 2007 Jun;**169**,1239–1260.

Refereed publications using data from this loan

- Ágústsdóttir, T., Woods, J., Greenfield, T., Green, R. G., White, R. S., Winder, T., Brandsdóttir, B., Steinhórsson, S. & Soosalu, H. (2016). Strike-slip faulting during the 2014 Bárðarbunga-Holuhraun dike intrusion, central Iceland. *Geophysical Research Letters*, plus Supplementary Information, 43, 1495–1503, doi: 10.1002/2015GL067423
- Caudron, C., White, R. S., Green, R. G., Woods, J., Ágústsdóttir, T., Donaldson, C., Greenfield, T., Rivalta, E. & Brandsdóttir, B. Seismic amplitude ratio analysis of the Bárðarbunga-Holuhraun dike propagation and eruption, *Journal of Geophysical Research*, in press.
- Green, R.G., White, R.S. & Greenfield, T. (2014). Bookshelf faulting in the north Iceland volcanic rift zone, *Nature Geoscience*, 7, 29–33, plus Supplementary Information, doi: 10.1038/NGEO2012
- Green, R. G., Greenfield, T. & White, R. S. (2015). Triggered earthquakes suppressed by an evolving stress shadow from a propagating dyke, *Nature Geoscience*, 8, 629–632, doi: 10.1038/NGEO2491
- Green, R. G., Priestley, K. F. & White, R. S. (2017). Ambient noise tomography reveals upper crustal structure of Icelandic rifts, *Earth and Planetary Science Letters*, 466, 20–31, doi: 10.1016/j.epsl.2017.02.039
- Greenfield, T. & White, R. S. (2015). Building Icelandic igneous crust by repeated melt injections, *Journal of Geophysical Research*, doi: 10.1002/2015JB012009
- Greenfield, T., White, R. S. & Roecker, S. (2016). The magmatic plumbing system of the Askja central volcano, Iceland as imaged by seismic tomography, *Journal of Geophysical Research*, 121, doi: 10.1002/2016JB013163
- Hudson, T. S., White, R. S., Greenfield, T., Ágústsdóttir, T., Brisbourne, A. & Green, R. G. (2017). Deep crustal melt plumbing of Bárðarbunga volcano, Iceland, *Geophysical Research Letters*, 44, doi: 10.1002/2017GL074749
- Jenkins, J. S., Cottaar, S., White, R. S. & Deuss, A. (2016). Depressed mantle discontinuities beneath Iceland: Evidence of a garnet controlled 660 km discontinuity? *Earth and Planetary Science Letters*, 433 (2016) 159–168, doi: 10.1016/j.epsl.2015.10.053
- Jenkins, J., Maclennan, J., Green, R. G., Cottaar, C. & White, R. S. Crustal formation on a spreading ridge above a mantle plume: receiver function imaging of the Icelandic crust, *Journal of Geophysical Research, Solid Earth*, submitted.
- Pugh, D. J., White, R.S. & Christie, P.A.F. (2016). Automatic Bayesian polarity determination, *Geophysical Journal International*, doi: 10.1093/gji/ggw146
- Pugh, D. J., White, R.S. & Christie, P.A.F. (2016). A Bayesian method for microseismic source inversion, *Geophysical Journal International*, doi: 10.1093/gji/ggw186
- Sigmundsson, Freysteinn, Hooper, Andy, Hreinsdóttir, Sigrún, Vogfjörð, Kristín, Ófeigsson, Benedikt, Heimisson, Elías Rafn, Dumont, Stéphanie, Parks, Michelle, Spaans, Karsten, Guðmundsson, Gunnar B., Drouin, Vincent, Árnadóttir, Thóra, Jónsdóttir, Kristín, Guðmundsson, Magnús Tumi, Högnadóttir, Thórdís, Friðriksdóttir, Hildur María, Hensch, Martin, Einarsson, Páll, Magnússon, Eyjólfur, Samsonov, Sergey, Brandsdóttir, Bryndís, White, Robert S., Ágústsdóttir, Thorbjörg, Greenfield, Timothy, Green, Robert G. et al. (2015). Segmented lateral dyke growth in a rifting event at Bárðarbunga volcanic system, Iceland, *Nature*, 517, 191–195, doi:10.1038/nature14111

PhD Dissertations

- | | |
|---------------------|---|
| 2015 David Pugh | Bayesian source inversion of microseismic events |
| 2016 Tim Greenfield | The velocity structure and micro-seismicity of Askja central volcano, Iceland |
| 2016 Robert Green | The structure and seismicity of Icelandic rifts |
| 2017 Jenny Jenkins | Mantle interfaces beneath Iceland |

Conference Abstracts

We have published over 100 conference abstracts using the seismometers from this loan, and there is not space here to list them all. But the results are contained in the theses and refereed publications listed above which are all publicly available.

Table of instrument deployment details and locations during September 2014 when the deployment reached its maximum extent. Seismometers were moved around for operational reasons throughout the duration of the experiment, so the particular sensor at any given site may have varied through the project, and some sites were not occupied continuously. Sensors are Guralp 6TDs unless otherwise indicated.

Station Code	Lat	Long	Alt	INST	Sensor
ASK	65.05194	-16.64806	955	4	6355
BJK	64.46891	-16.75267	1572	16	6159
BRUN	65.20461	-16.86597	536	16	6D73
DALR	65.07733	-16.9367	801	16	6132
DREK	65.04944	-16.59703	820	4	6305
DSAN	64.92149	-16.72847	705	16	6037
DYFE	65.1055	-16.92232	710	4	6359
DYSA	64.9349	-16.6755	688	16	6108
DYN	64.79086	-17.36648	1145	3T	3Z76
EFJA	65.03362	-16.96191	883	16	6010
FLAT	65.18279	-16.49796	728	16	6041
FLAE	64.85661	-16.94212	769	16	6051
FLUR	64.84354	-17.02693	838	ESP	4849
FYDU	64.87353	-16.91978		16	6070
GODA	65.03704	-16.85982	1266	4	6150
HELI	65.19875	-16.21843	491	16	6166
HETO	65.1287	-16.31698	581	16	6161
HOTT	65.04748	-16.52985	718	16	6135
HRIM	64.89633	-16.97921	849	16	6575
HRUR	65.15577	-16.67551	697	16	6177
HVAM	65.30373	-16.69773	583	16	6208
JONS	65.07747	-16.8057	1174	16	6D75
KATT	64.99901	-16.96339	885	16	6098
KLUR	65.07529	-16.75322	1114	16	6D74
KODA	65.36317	-16.84383	517	ESP	6800
KOLL	65.29024	-16.56726	593	ESP	6797
KVER	64.76347	-16.61068	829	16	6D80
LAUF	64.02918	-18.13262	563	ESP	6442

LIND	64.85278	-16.4523	726	ESP	6794
LOGR	65.15841	-16.82334	730	16	6D81
LOKT	65.13623	-16.91511	630	ESP	6380
MIDF	65.08676	-16.32961	572	16	6212
MOFO	64.9844	-16.65119	702	16	6D77
MYVO	65.1555	-16.36895	639	16	6D76
NAUG	65.02023	-16.57285	697	16	6017
NOFL	64.92377	-16.83372	741	16	6211
NOHR	64.93392	-16.94952	826	4	6024
OSKV	65.03933	-16.70164	1209	4	6026
RIFR	64.91533	-16.37127	657	16	6D82
RIMA	64.90194	-16.88503	748	16	6186
RJUP	64.74295	-17.52738	996	16	6J81
RODG	64.98513	-16.88639	1022	16	6200
SKAF	64.02609	-16.98853	259	16	6197
SOFA	64.97894	-16.83757	1004	4	6096
SOSU	64.94193	-16.8543	805	16	6036
STAM	64.99691	-16.80959	1171	16	6103
STJA	64.81091	-16.53488	751	16	6086
STOR	65.13313	-16.63144	721	4	6173
SVAD	65.11746	-16.57498	680	16	6128
SVIN	64.3866	-15.39449	40	ESP	6318
SYLG	64.42524	-18.1097	899	ESP	7880
TOHR	64.91658	-16.78473	715	16	6116
TUNG	64.80818	-17.9328	888	16	6021
URDU	64.82033	-17.14737	1002	16	6038
UTYR	65.03605	-16.31867	623	16	6087
VADA	64.99487	-16.53817	673	16	6145
VEGG	65.38205	-16.37467	507	16	6163
VIFE	65.0845	-16.4935	696	16	6D79
VIKS	65.06013	-16.4136	641	16	6192
VONK	64.67315	-17.75591	1011	ESP	6796
VSH	64.80775	-15.72768	860	ESP	6443